Atmos. Meas. Tech. Discuss., 4, 2037–2069, 2011
www.atmos-meas-tech-discuss.net/4/2037/2011/
doi:10.5194/amtd-4-2037-2011

Atmospheric Measurement Techniques Discussions

Remote sensing of aerosols by using polarized, directional and spectral measurements within the A-Train: the PARASOL mission

D. Tanré[1], F. M. Bréon[2], J. L. Deuzé[1], O. Dubovik[1], F. Ducos[1], P. François[1], P. Goloub[1], M. Herman[1], A. Lifermann[3], and F. Waquet[1]

[1]Laboratoire d'Optique Atmosphérique, CNRS-INSU UMR 8518, Université de Lille 1, Villeneuve d'Ascq, France
[2]LSCE, CEA, Gif sur Yvette, France
[3]Centre National d'Etudes Spatiales, Toulouse, France

Received: 16 March 2011 – Accepted: 19 March 2011 – Published: 1 April 2011

Correspondence to: D. Tanré (didier.tanre@univ-lille1.fr)

Published by Copernicus Publications on behalf of the European Geosciences Union.

Abstract

The aerosol remote sensing from space has started in the 1980's using observations provided by geostationary satellites or by polar orbiting platforms not specifically designed for observing aerosols. As a result, the number of retrieved parameters was limited and retrievals in the visible restricted over ocean. Over land, because of the important surface contribution, the aerosol detection was performed in the UV (or in the dark blue) where most of the earth surfaces are dark enough but with overlap of multiple aerosols parameters, content, altitude and absorption. Instruments dedicated to aerosol monitoring are recently available and the POLDER instrument on board the PARASOL mission is one of them. By measuring the wavelength, angular and polarization properties of the radiance at the top of the atmosphere, in coordination with the other A-Train instruments, PARASOL can better quantify aerosol optical depths (AOD) and improve the derivation of the radiative and physical properties. The instrument, the inversion schemes and the list of aerosol parameters are described. Examples of retrieved aerosol parameters are provided as well as innovative approaches and further inversion techniques.

1 Introduction

Atmospheric aerosols interact with solar and thermal radiation. By scattering sunlight and reflecting a fraction of it back to space, aerosols first cool the atmosphere-surface system; the resulting effect is named the aerosol direct (or parasol) effect. By absorbing sunlight in the atmosphere, they further cool the surface but warm the atmosphere. As a result, they change the temperature and humidity profiles and the conditions for cloud development; this is the semi-direct effect. They also impact the cloud properties by acting as cloud condensation nuclei and ice nuclei. They modify the cloud droplet concentration and tend to decrease the droplet size with potential impact on precipitation,

AMTD
4, 2037–2069, 2011

which is named the indirect effects (see, for example, Hansen et al., 1997; Ramanathan et al., 2001).

For estimating the aerosol forcing on the climate, there is a need for discriminating man-made aerosols and those resulting from natural processes. If in situ chemical measurements are required for definite identification, there are other means to retrieve the aerosol origin. For instance, the aerosol size distribution includes several modes that are associated with specific physical or chemical processes. The fine (or accumulation) mode, around roughly 0.1–0.2 µm, is formed from condensation or chemical conversion of gases to the liquid phase. From satellite, it is clear that anthropogenic aerosols downwind from vegetation fires and industrial pollution regions are characterized by high concentration of fine particles. When fine particles are emitted by natural process, they display much smaller spatial variability as confirmed by transport models (Chin et al., 2002). Natural aerosol particles, wind driven sea spray, wind blown dust and soil, fly ash and biogenic particles, are within the coarse mode with radius mainly larger than 1.0 µm. Particles size and spatial distribution can be used for separating natural from anthropogenic aerosols (Kaufman et al., 2002); the spectral absorption or the non-spherical fraction are also an indication of the aerosol type (see, for example, Kaufman et al., 2002; Dubovik et al., 2002).

To be used in climate models or for evaluating transport models (see, for example, Menon et al., 2002 and Chin et al., 2002), the knowledge of the aerosol distribution is required at a global scale on a daily basis with a resolution of 1-10 km, which can be only achieved using remote sensing from sun-synchronous satellites. The A-Train satellite formation (http://aqua.nasa.gov/doc/pubs/A-Train_Fact_sheet.pdf), which consists of presently five satellites flying in constellation, has been designed to study aerosol (Anderson et al., 2005), clouds and precipitation; the instruments within the A-Train specifically dedicated to aerosol monitoring and using the sunlight reflected by the Earth, are PARASOL/POLDER and AQUA/MODIS.

This paper provides a description of the PARASOL mission with a brief summary of the instrument, the list of the retrieved aerosol parameters illustrated by few examples.

AMTD
4, 2037–2069, 2011

Finally, enhancements expected by the use of more sophisticated inversion schemes, are given.

2 The PARASOL mission

PARASOL (Polarization and Anisotropy of Reflectances for Atmospheric Science coupled with Observations from a Lidar), decided in 1999, is the second microsatellite in the Myriade series, developed by CNES. It carries a POLDER-like (Polarization and Directionality of the Earth's Reflectances) wide-field radiometer. The instrument (Deschamps et al., 1994) measures the polarized light in different directions for retrieving with more accuracy the aerosol (as well as cloud) optical and physical properties. The mission takes also advantage of the other instruments in the A-Train formation, which for our objectives mainly include MODIS (MODerate resolution Imaging Spectroradiometer) (King et al., 1992) on the AQUA satellite (Parkinson, 2003) and the CALIOP lidar (Winker et al., 2009) on CALIPSO (Winker et al., 2003, 2010). Although the TERRA/MISR instrument is not part of the train and cannot be used in synergy with PARASOL, let us remind that it has also angular capabilities such as POLDER for deriving the AOD and aerosol type (Kahn et al., 2001).

2.1 The POLDER instrument

The POLDER instrument has flown on both the ADEOS-I and ADEOS-II platforms in 1996–1997 and 2003, respectively. Unfortunately, due to failure of the satellite solar panels, the measurement time series are limited to respectively 8 and 7 months. PARASOL platform was launched in December 2004 by the French Space Agency (CNES) in order to be part of the A-Train. It is routinely acquiring data since March 2005 and, as previoulsy stated, provides spectral, directional and polarized characteristics of the solar radiation reflected by the Earth-Atmosphere system. It has a sunsynchronous orbit with 01:30 p.m. ascending node at an altitude of 705 km.

AMTD
4, 2037–2069, 2011

The payload consists of a digital camera with a 274 × 242-pixel CCD detector array, wide-field telecentric optics and a rotating filter wheel enabling measurements in 9 spectral channels from blue (0.443 µm) through to near-infrared (1.020 µm). Polarization measurements are performed at 0.490 µm, 0.670 µm and 0.865 µm. The bandwith is between 20 nm and 40 nm depending on the spectral bands. The pixel size is 5.3 km × 6.2 km at nadir. Because it acquires a sequence of images every 20 s, the instrument can observe ground targets from different view directions, ±51° along track and ±43° across track. Compared to POLDER-I and II, the telecentric optics array has been turned 90° to favour multidirectional viewing over daily global coverage. Likewise, a 1020 nm waveband has been added to conduct observations for comparison with data acquired by the CALIOP lidar (Winker et al., 2009) on CALIPSO. PARASOL also relies on the innovative techniques (Hagolle et al., 1999) developed to calibrate in-flight the POLDER instruments. The method uses in particular the Sun's reflection from the ocean surface, clouds and desert areas as targets to validate the pre-flight performance (Fougnie et al., 2007). The temporal degradation of the sensor is monitored and corrected for in real time (Fougnie et al., 2009).

2.2 The A-Train

The present 5 satellites of the A-Train, including AQUA, AURA, CALIPSO, CLOUDSAT and PARASOL, cross the equator at around 01.30 p.m. LT (local time), a few minutes apart. Although each mission is fully autonomous and consistent by itself, their combination provides the opportunity to derive new parameters as well as to put additional constraints on the individual inversions.

AQUA is in orbit since 4 May 2002 and the first to cross the equator each day. Its mission is centered on the Earth's water cycle. MODIS sensor, which is the main sensor relevant for aerosol monitoring on AQUA, started collecting data in June 2002. It provides radiance measurements from 0.41 to 14 µm in 36 spectral bands very suitable for aerosol and cloud monitoring. The aerosol characteristics are derived at the

AMTD
4, 2037–2069, 2011

$10 \times 10\,km^2$ resolution over the ocean (Tanré et al., 1997) and land (Kaufman et al., 1997) using independent algorithms (Remer et al., 2005).

The Cloud-Aerosol Lidar and Infrared Pathfinder Satellite Observation (CALIPSO) satellite was launched in April 2006. The payload includes the CALIOP lidar (Cloud-Aerosol Lidar with Orthogonal Polarization), a passive Infrared Imaging Radiometer (IIR), and visible Wide Field Camera. An interesting feature of Mie scattering lidar is the depolarization ratio measurement, which is a good index of non-sphericity of the scatterers. It is used for detecting mineral dust particles. The present CALIOP algorithms used for aerosols have been described (Omar et al., 2005; Winker et al., 2009) and its ability to derive vertical structures demonstrated (see, for example, Vaughan et al., 2009).

3 The PARASOL data processing and the derived aerosol parameters

The parameters that are usually accessible from remote sensing are (i) the aerosol optical depth (AOD), that is a measure of the integrated aerosol load through the atmosphere valuable for evaluating aerosol amount and its variability and (ii) the Ångström Exponent (AE) related to the AOD spectral dependence that gives an indication of the column integrated aerosol size distribution. With POLDER and its polarized and directional signatures, in addition to the commonly spectral signature, it is possible over the ocean to better constrain the choice of models in the inversion algorithms and to determine the size and shape of particles. Over land for highly reflective surfaces, only polarization data are presently used. Our land retrieval scheme is based on the following findings: (i) the surface polarized reflectances are rather uniform and constant, (ii) the atmospheric contribution is larger than the surface polarized reflectance. Nevertheless, since polarization is mainly controlled by small particles, only the small (or accumulation) mode can be retrieved. This existing limitation will be overcome with the more sophisticated inversion scheme under development (Dubovik at al., 2010).

AMTD
4, 2037–2069, 2011

3.1 The algorithms

Algorithms have been developed to process the POLDER measurements in terms of aerosols parameters (Table 1) provided at $18.5 \times 18.5\,km^2$ resolution (3×3 pixels). Computations are based on the plan-parallel assumption and use the successive order of scattering method (Lenoble et al., 2007).

Over the ocean where the surface is dark, several aerosol parameters are derived using the inversion scheme developped by Deuzé et al. (1999) and Herman et al. (2005). The ocean reflectance is modelled with the Cox and Munk (1954) equations assuming a wind speed of 5m/s for considering the surface-atmosphere multiple interactions. The actual wind speed provided by the ECMWF weather forecast model is used in the glint mask and for computing the foam reflectance according to the Koepke's model (1984); the underwater contribution is taken equal to 0.001 and 0.000 at 670 and 865 nm respectively. The algorithm uses the total and polarized radiances at 670 and 865 nm and assumes that the size distribution follows a combination of two lognormal aerosol size distributions, one in the fine or accumulation mode (sub-micron size, effective radius r_{eff} typically smaller than 0.5 µm) and one in the coarse mode (r_{eff} typically larger than 1.0 µm). Non-absorbing particles are considered in both modes. The total radiance, L, at the satellite level is written,

$$L\,(\mu_s,\,\mu_v,\,\phi_v) \;=\; \eta\,L^{f}\,(\mu_s,\,\mu_v,\,\phi_v) \;+\; (1\;-\;\eta)\,L^{c}\,(\mu_s,\,\mu_v,\,\phi_v) \qquad (1)$$

where $L^f\,(\mu_s, \mu_v, \phi_v)$ and $L^c\,(\mu_s, \mu_v, \phi_v)$ are the radiances of the fine (f) and coarse (c) modes, respectively, $\mu_s = \cos(\theta_s)$ with θ_s the solar zenith angle, $\mu_v = \cos(\theta_v)$ for the viewing zenith angle θ_v, and ϕ_v the relative azimuth angle. Equation (1) (Wang and Gordon, 1994) assumes that the effect of the multiple scattering on the spectral radiance is independent on the size distribution. The retrieved parameters are reported in Table 1. In the coarse mode, spherical or non-spherical particles (as needed for saharan dust, see Volten et al., 2001) are considered and when the geometrical conditions are optimal, the shape of the particles is derived (Herman et al., 2005). The refractive index retrieval is attempted from the polarization measurements. If the real

AMTD
4, 2037–2069, 2011

part of the refractive index of the coarse mode is retrieved when spherical particles are present (generally close to 1.35, indicating hydrated particles), the derivation of the refractive index of the accumulation mode is still tentative. Let us add that PARASOL has at least one viewing direction out of the glint making aerosol AOD retrievals possible everywhere over water.

Over land surfaces, the PARASOL aerosol retrieval is based on polarized measurements L^{POL} (μ_s, μ_v, ϕ_v) at 670 and 865 nm (Herman et al., 1997b; Deuzé et al., 2001). Contrary to the total radiances, polarized reflectance of surfaces is small and fairly spectrally independent, although it does have a very strong directional signature (Nadal and Bréon, 1999; Maignan et al., 2009). Scattering by the spherical particles within the accumulation mode (radii less than about 0.5 µm) generates highly polarized light, which makes the polarized satellite radiances more subject to the presence of aerosols than the total radiances. So, the models used in the land algorithm are considering aerosols within the accumulation mode only and the contribution of the coarse mode is neglected (see Table 1). The refractive index is taken equal to 1.47–0.01 which corresponds to a mean value for aerosols resulting from biomass burning or pollution events (Dubovik et al., 2002). The surface contribution depends on the surface type, bare soils or vegetated areas and is estimated from a relationship using empirical coefficients adjusted for the different classes of land surfaces according to the main IGBP biotypes and the NDVI. Although larger aerosol particles, such as desert dust, almost do not polarize sunlight and are therefore hardly detected from polarization measurements, the coarse mode can contribute to the polarization for very intense events and may lead to misinterpretation of the retrieved AOD.

The aerosol models that are used in both cases, land and ocean, are described in the Appendix.

AMTD
4, 2037–2069, 2011

3.2 Validation

As noted, the AOD is the main aerosol parameter that is derived from space and needs to be validated from surface observations. There are several international networks that have extensive records of AOD measurements like AERONET, BSRN, GAW-PFR, and SKYNET but the long period of observations and the multi-site aspect of AERONET (Holben et al., 1998) with around 200 sunphotometers distributed around the world (Holben et al., 2001) make it very attractive as a validation tool.

Comparisons of total AOD's derived from POLDER with ground based AERONET measurements can be performed so far over ocean only. AERONET and POLDER-1 on ADEOS showed good agreement with typical RMS errors on the order of 0.05 with no significant bias (Goloub et al., 1999). For POLDER/PARASOL, Bréon et al. (2010) showed also a good correlation (0.91) but with a bias of around 0.03 which is not explained yet.

The fine-mode optical depth can also be compared to AERONET measurements. Over ocean, the performances are lower (correlation of 0.78) than for the total AOD (Bréon et al., 2010) partly due to some discrepancy in the aerosol radius cutoff. In the corresponding study, it is the standard value of AERONET cutoff ($r \leq 0.6\,\mu m$) which is used. Over land, Bréon et al. (2010) get a significant correlation (0.84) with the sunphotometer measurements. Again, the value of the cutoff can lead to an underestimation of the satellite retrieval compared to AERONET. Over land and in regions where dust-loaded atmospheres are excluded, i.e. in regions affected by biomass burning or pollution aerosols, particular comparisons with AERONET measurements show better results with no significant bias. A specific study (Fan et al., 2008) comparing AERONET data over Beijing and Xianghe in China demonstrated the capability of PARASOL for determining the anthropogenic contribution (particle radii less than or equal to 0.3 µm) of regional aerosols. Correlation between the two data sets gives a slope close to one and a 0.03 RMS on AOT when the contribution of the accumulation mode to the AOT at 865 nm is larger than 30%.

AMTD
4, 2037–2069, 2011

Angström exponents α over ocean were also compared in Goloub et al. (1999). Obviously, the accuracy on the Angström exponent is poor when the aerosol optical thickness is small. When comparisons are restricted to an aerosol optical thickness larger than 0.1 at 865 nm, the PARASOL α values allow the differentiation of the aerosol types.

3.3 Discussion

Are the differences between AERONET and PARASOL aerosol products understandable? First of all, when data set are limited to the "best observation conditions", i.e. spatial and temporal variations of the aerosol field discarded and consistency of the aerosol type over the time checked, both AOD's are in good agreement. It confirms that the assumptions (aerosol models of the LUT's, surface effects) used in the inversion algorithm itself are valid, as well as the forward computations. More discrepancies are observed when more comprehensive data sets are considered. There are several factors that can affect the satellite retrieval. Let us first point out that mis-calibration of the satellite sensor would result in a systematic bias but, based on our calibration error budget (Fougnie et al., 2007), it cannot explain the 0.03 value. Residual straylight may explain the biais and specific studies are under way.

Cloud screening may be more or less stringent and comparison of the operational products may be affected. For POLDER, the cloud screening (Bréon and Colzy, 1999) is based on thresholds on the total and polarized reflectances in different spectral bands, on the detection of the polarized rainbow corresponding to the presence of water droplets and on the spatial variability of reflectance (over ocean) and the pressure derived within the O_2 absorption band at 762 nm (over land). Based on on-going additional analysis using the CALIOP information, there are some thin cirrus that are not detected by the cloud screening and bias the aerosol products. We so far do not identify clever solutions to improve it with the present spectral coverage.

Retrieval accuracies of the AOD's are also different depending on the underlying surface, ocean or land. Over land, when the surface is bright, the aerosol remote

AMTD
4, 2037–2069, 2011

sensing requires more sophisticated approaches than over ocean since the sensitivity to the presence of aerosol decreases. The properties of the initial aerosol models are also more crucial over reflecting surfaces than over ocean; for instance the impact of the aerosol single scattering albedo is larger over bright surfaces. The impact of some external factors is also larger: cloud screening is more challenging over land and the uniformity of the aerosol field is more questionable close to the sources. In the case of PARASOL/POLDER over land, the AOD is resulting for the fine mode and is more challenging to validate since information on the aerosol size distribution is therefore needed. Over ocean, the problem is not so ill-conditioned but there are other issues. For instance, in presence of non-spherical particles, the spectral dependence of the radiance, that controls the size retrieval, is more similar to that of particles smaller than those really present. So the choice, and the number, of aerosol models used to build the Look-Up-Tables are crucial and impact the AOD and size retrievals.

The PARASOL archive is now large enough with 5 years of data to perform regional studies for assessing the inversion performances in different regions and for different atmospheric conditions.

4 Some illustrations

The PARASOL results hereinafter are focused on two aerosol parameters that are illustrating the unique capabilities of the sensor: (i) the AOD due to non-spherical particles over ocean and (ii) the AOD of the accumulation mode available over land and ocean.

4.1 Non-spherical aerosols over the ocean

The optical depths of the non-spherical coarse mode over the ocean are averaged over the seasons of the five complete years of data presently available. On Fig. 1, rows represent the AOD for the four seasons of a given year, spring, summer, autumn and winter from the left to the right respectively, starting in spring 2005 (top left) and ending

AMTD
4, 2037–2069, 2011

in winter 2010 (bottom right). Figure 1 shows that non-spherical particles, associated essentially to the presence of mineral dust, is a major component of the aerosols over the ocean. Let us point out that our analysis is not biased by the presence of other aerosol types like smoke in the winter from the Sahel over the Golf of Guinea or in the summer from the South-Western African region since spherical fine or large particles are excluded.

Over the Atlantic ocean, we observe the well-known general patterns of spatial and temporal distributions of Saharan Dust outbreaks (Husar et al., 1997; Kaufman et al., 2005). In winter time (right column), dust is transported over the Gulf of Guinea and is reaching the coast of Brazil in South America. The inter-annual variability can also be observed with low contents in 2006 (December 2005/January 2006/February 2006) and 2010 (December 2009/January 2010/February 2010) when 2007, 2008 and 2009 are dustier. Again, there is no misinterpretation of our results due to the possible presence of smoke in the area. In the summer (2nd column from the left), since the latitudinal variation is controlled by the movement of the West African mid-tropospheric jet (Carlson and Prospero, 1972), the dust belt is in its northern most position (20° N) and reaches the Caribbean islands and Florida with large year-to-year variations. In the autumn (3rd column from the left), most of the Atlantic Ocean is free of aerosols with the presence of dust limited to areas close to the African continent. In spring (1st column), dust is also transported across the Atlantic Ocean to the Amazon Basin like in winter but above, instead of below, the equator and with higher concentrations. For the Arabia sea and the Bay of Bengal, the seasonnal variation is similar to that for the Atlantic ocean with smaller contents and a larger extent in 2008 and 2009 compared to the other years. Over the Pacific Ocean, the northern part is more affected by dust that the southern part. There is a strong seasonal cycle with the presence of plumes in spring (MAM) that reach the West Coast of the United States. The PARASOL capability to discriminate spherical and non-spherical particles is very valuable in this region where dust is mixed with other aerosol types, depending on the season.

AMTD
4, 2037–2069, 2011

4.2 Aerosol optical thickness anomaly of the accumulation mode over land and ocean for (September-October-November)

Aerosol optical thickness anomalies for the 5 years are compared with the 2005–2009 mean values in Fig. 2. We selected the autumn season when the number of fires is expected to be maximum in the tropical regions as reported by the high values of the AOD over Brazil, South Africa and Indonesia (Fig. 2a); high values not related to Biomass Burning are also observed in the north part of India and East of China (Fig. 2a). Figure 2b to f show the interannual variations over the 5 years from March 2005 to February 2010 respectively.

Lower concentrations are reported over Africa in 2006 (Fig. 2c) as well as in 2008 (Fig. 2e) and 2009 (Fig. 2f) over South America and Indonesia. On the other hand, large concentrations are observed in Indonesia in 2006 and over Brazil in 2007 (Fig. 2d) and to a less extend in 2005 (Fig. 2b). Our results are in good agreement with other studies using MODIS already in 2008 (Remer et al., 2008) or more recently using OMI (Torres et al., 2010).

The causes of these fluctuations are multiple: (i) changes in intensity and number of fires or controls of pollutant emissions, (ii) changes in meteorological fields that affect aerosol transport or (iii) changes in scavenging processes, precipitations or dry deposition. Compared to OMI or/and MODIS, PARASOL selects the aerosol fine mode resulting from anthropogenic activities and is sensitive equally to pollution events and smoke. The puzzle can be solved by using inverse modeling to retrieve the global aerosol source emissions as explained in Dubovik et al. (2008).

5 Further developments

The PARASOL measurements are sensitive to several parameters of the aerosol model: the size distribution, the real and imaginary parts of the refractive index, the particle shape, and the altitude of the aerosol layer (see e.g. Deuzé et al., 2001; Herman

AMTD
4, 2037–2069, 2011

et al., 2005; Mishchenko et al., 2007; Chowdhary et al., 2001; Hasekamp, 2010). The present algorithms, as described in Sect. 3, do not use the whole data set because the basic LUT approach for the inversion is not sophisticated enough for considering all the variables as one. In this section, we first illustrate the potentiality of the PARASOL data for discriminating absorption and altitude of the aerosol layer using both the total and polarized radiances. Then, a short description of the upcoming algorithms is provided. Finally, the unique capability of passive sensors like PARASOL to detect the presence of an aerosol layer above a cloud deck and to estimate its AOD, as described in Waquet et al. (2009), is again pointed out.

5.1 Altitude/absorption

Over land, in the UV, most of the earth surfaces are dark and the spectral ratio of radiances, called the Aerosol Index "AI", in two UV channels of the TOMS/OMI series instruments were found to be sensitive to the presence of elevated smoke or dust layers above scattering atmosphere (Herman et al., 1997a). The use of AI is widespread since it is a satellite product that provides aerosol information at a global scale (and over deserts) over a large period of time. CALIPSO and MISR are also attractive but their daily spatial coverage is more limited. In a similar way, it was suggested to use the bluest channel of MODIS (Hsu et al., 2006) for solving the surface contamination over surfaces reflecting in the visible. Nevertheless, the analysis in terms of aerosol content is not obvious since the altitude and the absorption of the aerosol layer are both impacting the AI (Herman et al., 1997a). We hereinafter illustrate the improvements brought by PARASOL by using polarization measurements at 0.490 µm in connection with total radiances.

The present aerosol algorithm over land is based on a best fit between polarized measurements at 0.670 µm and 0.865 µm and LUTs simulated for aerosols within the accumulation mode (see Sect. 3.1 and Appendix). In the algorithm, aerosols and molecules are vertically distributed with height scales of 2 and 8 km respectively and one value of the aerosol absorption is considered. If the vertical repartition has no

AMTD
4, 2037–2069, 2011

strong impact on polarized reflectances at 0.670 µm and 0.865 µm since the molecular optical thickness is low in the red and NIR, it is not anymore true at 0.490 µm. Likewise, the total radiances in the blue are impacted by both aerosol absorption and vertical repartition.

Figure 3 shows that the problem is actually rather one well-posed problem as soon as polarization measurements are considered. For standard observations, scattering angle of 102° and an aerosol effective radius of 0.2 µm, we consider several aerosol vertical repartitions and different values of the imaginary part of the refractive index, from 5.0×10^{-3} to 3.0×10^{-2} which correspond to a single scattering albedo between 0.974 and 0.860 respectively. The aerosol layer is supposed to follow a rectangular step function of 1 km width and is identifed by the value of half-maximum, 0.5 km, 1.5 km, etc. Double-lines represent the total radiances that would be measured for one value of the absorption and different altitude layers, solid lines the polarized radiances that would be measured for one value of the altitude layer and different absorptions. If both radiances are impacted by the two unknowns, it is the absorption that is the driving parameter for the radiances (double-lines are almost parallel to the y-axis) and the altitude for the polarized radiances (solid lines are almost parallel to the x-axis). The polarized radiances result from photons that are scattered once or two times, so absorption has a limited impact when the respective location of molecules and aerosols is important, aerosol layer "hiding" the molecular contribution coming from below. On the other hand, the total radiances are more depending on absorption when AOD is large enough with a limited impact of the vertical repartition except for grazing incidence or view direction. As a result, assuming that the aerosol model as well as the spectral dependence are estimated from measurements at 0.670 µm and 0.865 µm, the PARASOL polarized and total radiances in the bue can deconvolve the relative influences of altitude and absorption. Obviously, the accuracy of the retrieval is more questionnable when the aerosol content is decreasing.

This mask effect of molecular scattering by aerosols is an example of the basic physical process behind our statement that the PARASOL observations present sensitivity

AMTD
4, 2037–2069, 2011

to several aerosol parameters that are not accessible from unpolarized sensors (see Sect. 5.2).

5.2 Enhanced retrieval of aerosol properties

The PARASOL observations form the most comprehensive data set (spectral, directional and polarized radiances) currently available from space and provide an opportunity for more in-depth use of statistical optimization principles in satellite data inversion. As reported in Dubovik et al. (2010), the statistical optimization principles concept improves retrieval accuracy relying on pronounced data redundancy (excess of the measurements number over number of unknowns) that is not common in satellites observations.

As illustrated in Kokhanovsky et al. (2010), the PARASOL data associated with the sophisticated inversion algorithm (Dubovik, 2004; Dubovik et al., 2010) are the most efficient means for retrieving the properties of the aerosol model (a maritime aerosol model over ocean in the corresponding study) when compared with other sensors in a blind-test. The new method addresses important aspects of inversion optimization as accounting for errors in the input data, inverting multi-source data with different levels of accuracy, accounting for a priori and ancilliary information, estimating retrieval errors, clarifying potential of employing different mathematical inverse operations (e.g. comparing iterative versus matrix inversion), accelerating iterative convergence, etc. The algorithm includes additionally constraints on the retrieved surface properties, e.g. a priori constraints on the spectral variability of the parameters describing surface reflection (Dubovik et al., 2010), and simultaneously retrieves the surface reflectance together with aerosol properties.

The capability is illustrated in Fig. 4 extracted and adapted from Dubovik et al. (2010). It shows a preliminary comparison of AODs retrieved from PARASOL with coincident AERONET measurements over Banizoumbou, Niger, in January–February and in November–December 2009. The inversion is not perfect but is shown very promising since the retrieval of AOD over bright surfaces like deserts is the most challenging

AMTD
4, 2037–2069, 2011

objective. Additional sensitivity studies are under progress and improvement of the speed of the inversion is still required for applying the method operationnally to the 5 years of PARASOL data.

5.3 Aerosols above a cloud deck

Current aerosol retrievals from passive sensors are limited over cloud-free pixels, which can bias the estimate of aerosol direct effect as well as the retrieval of cloud properties from satellite. As emphasized in the document (http://aqua.nasa.gov/doc/pubs/A-Train_Fact_sheet.pdf), "combining the information from several sources gives a more complete answer to many questions than it would be possible from any single satellite taken by itself". The detection of the aerosol layer above the clouds is a great illustration of the concept.

PARASOL is providing two cloud top pressures (CTP), a "Rayleigh CTP" based on the polarization due to the molecules that are above the cloud (Goloub et al., 1994) and a "O_2 CTP" based on differential absorption measurements in two oxygen A-band at 760 nm (Vanbauce et al., 2003) when MODIS measurements provide an "IR CTP" in the thermal infrared channels (Menzel et al., 2008). It is the analysis of the CTP derived from the various methods, as well as their differences, that allows us to claim that it is possible to detect aerosols and retrieve the optical depth above a cloud with passive sensors such as PARASOL.

Discrepancies were observed between the three CTPs described above, which is not surprizing since the retrievals are based on different physical processes that are not exactly sensitive to the same altitude range. More surprizing was the behavior of the "Rayleigh CTP" over some regions: it was smaller than the two others, which was not anticipated and in conflict with our expectations. The corresponding areas were located in regions and time associated with the presence of aerosols in the fine mode, i.e. pollution and/or smoke generated mainly by anthropogenic activities. Waquet et al. (2009) have identified several cases over the subtropical South Atlantic ocean in August–September when fires occur in South-West Africa. They deeply analyzed

AMTD
4, 2037–2069, 2011

specific collocated POLDER/PARASOL, MODIS and CALIOP observations in 2006, from 14 to 18 August and found an "additional" polarization signal over the 90°–120° scattering angle range. This additional polarization leads the "Rayleigh" algorithm to underestimate the CTP, which was confirmed by the CALIOP data. The excess of polarization is due to the presence of an aerosol plume, as also confirmed by CALIOP observations. At this period of the year, fires in South-West Africa are frequent and meteorological processes favor biomass burning aerosols transport to the West. The AOD was retrieved from an approximate formulation of the cloud-aerosol interaction using single scattering approximation. The method is now improving with more accurate computations. Presence of dust cannot be handled with a similar approach but is under consideration using the polarized rainbow (Waquet el al., 2011).

6 Conclusions

The A-train with five satellites (AQUA, AURA, CALIPSO, CLOUDSAT, PARASOL) and more than four years of coincident data offers an unique archive for improving our knowledge of the optical, physical and radiative properties of clouds and aerosols. Its analysis will result in a better estimate of the cloud and aerosol radiative forcing and will contribute to the understanding of the aerosol indirect effect.

Data collected by PARASOL already allow to separate over the sea the fine aerosol component, mostly resulting from anthropogenic activities, from the coarse mode, mainly coming from natural processes; it is the first step to describe the aerosol direct forcing at the top and bottom of the atmosphere. The Angstrom coefficient, an indicator of particle size, is also deduced from the spectral optical thickness. Moreover, when the viewing geometry is suitable, PARASOL can discriminate large spherical marine aerosols from non-spherical desert aerosols, retrieve the effective radius of the accumulation and coarse modes and provide an estimate of the real part of the refractive index. Over land surfaces that are highly reflective, PARASOL is using the polarized radiance. If the surface contribution is reduced, polarization is mainly sensitive to the

AMTD
4, 2037–2069, 2011

presence of small particles, which allows us to derive the optical thickness of the fine mode only. The location, the strengths, the seasonal variability of the aerosol sources can be then monitored at a global scale.

Recent and future developments are even more appealing. The quantification of the direct effect of aerosol above clouds is now possible. With new algorithms presently under development, parameters such as the aerosol single scattering albedo, a key parameter for the semi-direct effect, will be retrieved.

Although each mission of the A-Train is fully autonomous and consistent by itself, their combination provides the opportunity to derive, to compare, to validate new parameters as well as to put additional constraints on inversion scheme. The set of observations is expected to better understand the processes related to climate change and PARASOL can provide several aerosol and cloud parameters needed for deeper analysis of the complex aerosol direct, semidirect and indirect effects.

Appendix A

Description of the PARASOL aerosol models

We assume that the size distribution has two modes, fine and coarse, each of them follows a lognormal law defined by Eq. (A1)

$$n(r) = \frac{dN}{dr} = \frac{n_0}{\sigma_0 \, r_0 \, \sqrt{2\,\pi}} \exp\left[-\frac{(\ln r - \ln r_0)^2}{2\,\sigma_0^2}\right] \quad \text{(A1)}$$

where n_0 is the density number, r_0 the median (or modal) radius and σ_0 the standard deviation of $\ln r$. The effective radius is defined by Eq. (A2).

$$r_{\text{eff}} = \int_0^\infty r^3 \, n(r) \, dr \Big/ \int_0^\infty r^2 \, n(r) \, dr = r_0 \exp\left(2.5\,\sigma_0^2\right) \quad \text{(A2)}$$

AMTD
4, 2037–2069, 2011

The parameters of the log-normal size distribution as well as the values of the refractive index used to build the LUT are reported in Tables A1 and A2 for ocean and land retrieval respectively.

List of abbreviations

ADEOS	Advanced Earth Observing System
AERONET	AErosol RObotic NETwork
BSRN	Baseline Surface Radiation Network
CALIOP	Cloud-Aerosol Lidar with Orthogonal Polarization
CALIPSO	Cloud-Aerosol Lidar and Infrared Pathfinder Satellite Observation
CLOUDSAT/CPR	Cloud Profiling Radar
GAW-PFR	Global Atmosphere Watch – Precision Filter Radiometer
MISR	Multi-angle Imaging Spectro-Radiometer
MODIS	MODerate resolution Imaging Spectrometer
OMI	Ozone Measuring Instrument
PARASOL	Polarization and Anisotropy of Reflectances for Atmospheric Sciences coupled with Observations from a Lidar
POLDER	POLarization and Directionality of the Earth's Reflectances
SKYNET	Observation network of sky radiometers located in the Eastern Asia
TOMS	Total Ozone Mapping Spectrometer.

Acknowledgements. The authors thank all those who have contributed to the PARASOL project mainly at the CNES_CCC (Centre de Commande Contrôle), CNES_CPP (Centre de Production POLDER) and CNES_SQI (Système Qualité Image PARASOL). The authors are also thankful to CNRS-INSU, CNES/DSP, University Lille 1 and Région Nord-Pas de Calais for their support. Alexander Kokhanovsky is acknowledged for his support. The PARASOL level 1 data are available from http://polder.cnes.fr/. PARASOL level-2 and Level-3 products, browse images as well as data from some other A-Train sensors are available from the ICARE data center

AMTD
4, 2037–2069, 2011

(http://www.icare.univ-lille1.fr/parasol/). The authors thank the ICARE Data and Services Center for providing access to the PARASOL data and for general assistance and development support. The publication of this article is financed by CNRS-INSU.

The publication of this article is financed by CNRS-INSU.

References

Anderson, T. L., Charlson, R. J., Bellouin, N., Boucher, O., Chin, M., Christopher, S. A., Haywood, J., Kaufman, Y., Kinne, S., Ogren, J. A., Remer, L. A., Takemura, T., Tanré, D., Torres, O., Trepte, C. R., Wielicki, B. A., Winker, D. M., and Yu, H.: An "A-Train" Strategy for Quantifying Direct Climate Forcing by Aerosols, B. Am. Meteorol. Soc., 86, 1795–1809, 2005.

Bréon, F. M. and Colzy, S.: Cloud detection from the spaceborne POLDER instrument and validation against surface synoptic observations, J. Appl. Meteorol., 38, 777–785, 1999.

Bréon, F. M., Vermeulen, A., and Descloitres, J.: An evaluation of satellite aerosol products against sunphotometer measurements, Remote Sens. Environ., in press, 2011.

Carlson, T. N. and Prospero, J. M.: The large scale movement of Saharan air outbreaks over the Northern equatorial Atlantic, J. Appl. Meteorol., 11, 283–297, 1972.

Chin, M., Ginoux, P., Kinne, S., Torres, O., Holben, B. N., Duncan, B. N., Martin, R. V., Logan, J. A., Higurashi, A., and Nakajima, T.: Tropospheric aerosol optical thickness from the GOCART model and comparisons with satellite and sun photometer measurements, J. Atmos. Sci., 59, 461–483, 2002.

Chowdhary, J., Cairns, B., Mishchenko, M., and Travis, L.: Retrieval of aerosol properties over the ocean using multispectral and multiangle photopolarimetric measurements from the Research Scanning Polarimeter, Geophys. Res. Lett., 28, 243–246, 2001.

AMTD
4, 2037–2069, 2011

Cox, C. and Munk, W.: Measurement of the Roughness of the Sea Surface from Photographs of the Sun's Glitter, J. Opt. Soc. Am., 44, 838–850, 1954.
Deschamps, P. Y., Bréon, F. M., Leroy, M., Podaire, A., Sèze, G., and Bricaud, A.: The POLDER mission: Instrument characteristics and scientific objectives, IEEE T. Geosci. Remote, 32, 598–615, 1994.
Deuzé, J. L., Herman, M., Goloub, P., Tanré, D., and Marchand, A.: Characterization of aerosols over ocean from POLDER/ADEOS-1, Geophys. Res. Lett., 26, 1421–1424, 1999.
Deuzé, J. L., Bréon, F. M., Devaux, C., Goloub, P., Herman, M., Lafrance, B., Maignan, F., Marchand, A., Nadal, F., Perry, G., and Tanré, D.: Remote sensing of aerosols over land surfaces from POLDER-ADEOS-1 polarized measurements, J. Geophys. Res., 106, 4913–4926, 2001.
Dubovik, O.: Optimization of Numerical Inversion in Photopolarimetric Remote Sensing, in: Photopolarimetry in Remote Sensing, edited by: Videen, G., Yatskiv, Y., and Mishchenko, M., Kluwer Academic Publishers, Dordrecht, The Netherlands, 65–106, 2004.
Dubovik, O., Holben, B. N., Eck, T. F., Smirnov, A., Kaufman, Y. J., King, M. D., Tanré, D., and Slutsker, I.: Climatology of aerosol absorption and optical properties in key worldwide locations, J. Atmos. Sci. , 59, 590–608, 2002.
Dubovik, O., Lapyonok, T., Kaufman, Y. J., Chin, M., Ginoux, P., Kahn, R. A., and Sinyuk, A.: Retrieving global aerosol sources from satellites using inverse modeling, Atmos. Chem. Phys., 8, 209–250, doi:10.5194/acp-8-209-2008, 2008.
Dubovik, O., Herman, M., Holdak, A., Lapyonok, T., Tanré, D., Deuzé, J. L., Ducos, F., Sinyuk, A., and Lopatin, A.: Statistically optimized inversion algorithm for enhanced retrieval of aerosol properties from spectral multi-angle polarimetric satellite observations, Atmos. Meas. Tech. Discuss., 3, 4967–5077, doi:10.5194/amtd-3-4967-2010, 2010.
Fan, X., Goloub, Ph., Deuzé, J.-L., Chen, H., Zhang, W., Tanré, D., and Li, Z.: Evaluation of PARASOL aerosol retrieval over North East Asia, Remote Sens. Environ., 112, 697–707, 2008.
Fougnie, B. and Bach, R. : Monitoring of Radiometric Sensitivity Changes of Space Sensors Using Deep Convective Clouds: Operational Application to PARASOL, IEEE T. Geosci. Remote, 47, 851–861, 2009.
Fougnie, B., Bracco, G., Lafrance, B., Ruffel, C., Hagolle, O., and Tinel, C.: PARASOL in-flight calibration and performance, Appl. Optics, 46, 5435–5451, 2007.

AMTD
4, 2037–2069, 2011

Goloub, P., Deuzé, J.-L., Herman, M., and Fouquart, Y.: Analysis of the POLDER polarization measurements performed over cloud covers, IEEE T. Geosci. Remote, 32, 78–88, 1994.
Goloub, P., Tanré, D., Deuzé, J. L., Herman, M., Marchand, A., and Bréon, F. M.: Validation of the first algorithm applied for deriving the aerosol properties over the ocean using the POLDER/ADEOS measurements, IEEE T. Geosci. Remote, 37, 1586–1596, 1999.
Hagolle, O., Goloub, P., Deschamps, P. Y., Cosnefroy, H., Briottet, X., Bailleul, T., Nicolas, J. M., Parol, F., Lafrance, B., and Herman, M.:Results of POLDER in-flight calibration, IEEE T. Geosci. Remote, 37, 1550–1566, 1999.
Hansen, J., Sato, M., and Ruedy, R.: Radiative forcing and climate response, J. Geophys. Res., 102, 6831–6864, 1997.
Hasekamp, O. P.: Capability of multi-viewing-angle photo-polarimetric measurements for the simultaneous retrieval of aerosol and cloud properties, Atmos. Meas. Tech., 3, 839–851, doi:10.5194/amt-3-839-2010, 2010.
Herman, J. R., Bhartia, P. K., Torres, O., Hsu, C., Seftor, C., and Celarier, E.: Global distribution of UV-absorbing aerosol from Nimbus-7/TOMS data, J. Geophys. Res., 102, 16911–16922, 1997a.
Herman, M., Deuzé, J. L., Devaux, C., Goloub, P., Bréon, F. M., and Tanré, D.: Remote Sensing of Aerosols over Land Surfaces Including Polarization Measurements: Applications to POLDER Measurements, J. Geophys. Res., 102, 17039–17050, 1997b.
Herman, M., Deuzé, J. L., Marchand, A., Roger, B., and Lallart, P.: Aerosol Remote Sensing from POLDER/ADEOS over the Ocean. Improved Retrieval using Non-Spherical Particle Model, J. Geophys. Res., 110, D10S02, doi:10.1029/2004JD004798, 2005.
Holben, B. N., Eck, T. F., Slutsker, I., Tanré, D., Buis, J. P., Setzer, A., Vermote, E., Reagan, J. A., Kaufman, Y. J., Nakajima, T., Lavenu, F., Jankowiak, I., and Smirnov, A.: AERONET – A federated instrument network and data archive for aerosol characterization, Remote Sens. Environ., 66, 1–16, 1998.
Holben, B. N., Tanré, D., Smirnov, A., Eck, T. F., Slutsker, I., Abuhassan, N., Newcomb, W. W., Schafer, J. S., Chatenet, B., Lavenu, F., Kaufman, Y. J., Castle, J. V., Setzer, A., Markham, B., Clark, D., Frouin, R., Halthore, R., Karneli, A., O'Neill, N. T., Pietras, C., Pinker, R. T.,Voss, K., and Zibordi, G.: An emerging ground-based aerosol climatology: Aerosol optical depth from AERONET, J. Geophys. Res., 106, 12067–12097, 2001.
Hsu, N. C., Tsay, S.-C., King, M. D., and Herman, J. R.: Deep blue retrievals of Asian aerosol properties during ACE-Asia, IEEE T. Geosci. Remote, 44, 3180–3195, 2006.

AMTD
4, 2037–2069, 2011

Husar, R. B., Prospero, J., and Stowe, L. L.: Characterization of tropospheric aerosols over the oceans with the NOAA AVHRR optical thickness operational product, J. Geophys. Res., 10, 16889–16909, 1997.
Kahn, R. A., Banerjee, P., and McDonald, D.: The sensitivity of multiangle imaging to natural mixtures of aerosols over ocean, J. Geophys. Res., 106, 18219–18238, 2001.
Kaufman, Y. J., Tanré, D., Remer, L., Vermote, E., Chu, A., and Holben, B.: Operational remote sensing of tropospheric aerosol over land from EOS moderate resolution imaging spectroradiometer, J. Geophys. Res., 102, 17051–17067, 1997.
Kaufman, Y. J., Tanré, D., and Boucher, O.: A satellite view of aerosols in the climate system, Nature, 419, 215–223, 2002.
Kaufman, Y. J., Koren, I., Remer, L. A., Tanré, D., Ginoux, P., and Fan, S.: Dust transport and deposition observed from the Terra-Moderate Resolution Imaging Spectroradiometer (MODIS) spacecraft over the Atlantic Ocean, J. Geophys. Res., 110, D10S12, doi:10.1029/2003JD004436, 2005.
King, M., Kaufman, Y., Menzel, P., and Tanré, D.: Remote sensing of Cloud, Aerosol and Water Vapor properties from the Moderate Resolution Imaging Spectrometer (MODIS), IEEE T. Geosci. Remote, 30, 2–27, 1992.
Koepke, P.: Effective reflectance of the oceanic whitecaps, Appl. Optics, 23, 1816–1824, 1984.
Kokhanovsky, A. A., Deuzé, J. L., Diner, D. J., Dubovik, O., Ducos, F., Emde, C., Garay, M. J., Grainger, R. G., Heckel, A., Herman, M., Katsev, I. L., Keller, J., Levy, R., North, P. R. J., Prikhach, A. S., Rozanov, V. V., Sayer, A. M., Ota, Y., Tanré, D., Thomas, G. E., and Zege, E. P.: The inter-comparison of major satellite aerosol retrieval algorithms using simulated intensity and polarization characteristics of reflected light, Atmos. Meas. Tech., 3, 909–932, doi:10.5194/amt-3-909-2010, 2010.
Lenoble, J., Herman, M., Deuzé, J. L., Lafrance, B., Santer, R., and Tanré, D.: A Successive Order of Scattering Code for Solving the Vector Equation of Transfer in the Earth's Atmosphere with Aerosols, J. Quant. Spectrosc. Ra., 107, 479–507, 2007.
Maignan, F., Bréon, F.-M., Fédèle, E., and Bouvier, M.: Polarized reflectances of natural surfaces: Spaceborne measurements and analytical modeling, Remote Sens. Environ., 113, 2642–2650, 2009.
Menon, S., DelGenio, A. D., Koch, D., and Tselioudis, G.: GCM Simulations of the Aerosol Indirect Effect: Sensitivity to Cloud Parameterization and Aerosol Burden, J. Atmos. Sci., 59, 692–713, 2002.

AMTD
4, 2037–2069, 2011

Menzel, W. P., Frey, R. A., Zhang, H., Wylie, D. P., Moeller, C. C., Holz, R. E., Maddux, B., Baum, B. A., Strabala, K. I., and Gumley, L. E.: MODIS global cloud-top pressure and amount estimation: Algorithm description and results, J. Appl. Meteorol. Clim., 47, 1175–1198, 2008.

Mishchenko, M. I., Cairns, B., Kopp, G., Schueler, C. F., Fafaul, B. A., Hansen, J. E., Hooker, R. J., Itchkawich, T., Maring, H. B., and Travis, L. D.: Accurate monitoring of terrestrial aerosols and total solar irradiance: Introducing the Glory Mission, B. Am. Meteorol. Soc., 88, 677–691, doi:10.1175/BAMS-88-5-677, 2007.

Nadal, F. and Bréon, F. M.: Parameterization of surface polarized reflectance derived from POLDER spaceborne measurements, IEEE T. Geosci. Remote, 37, 1709–1718, 1999.

Omar, A. H., Won, J.-G., Winker, D. M., Yoon, S.-C., Dubovik, O., and McCormick, M. P.: Development of global aerosol models using cluster analysis of Aerosol Robotic Network (AERONET) measurements, J. Geophys. Res., 110, D10S14, doi:10.1029/2004JD004874, 2005.

Parkinson, C. L., Aqua: an Earth-Observing Satellite mission to examine water and other climate variables, IEEE T. Geosci. Remote, 41, 173–183, 2003.

Ramanathan, V., Crutzen, P., Kiehl, J., and Rosenfeld, D.: Aerosols, Climate, and the Hydrological Cycle, Science, 294, 2119–2124, 2001.

Remer, L. A., Kaurman, Y. J., Tanré, D., Mattoo, S., Chu, D. A., Martins, J. V., Li, R.-R., Ichoku, C., Levy, R. C., Kleidman, R. G., Eck, T. F., Vermote, E., and Holben, B.N.: The MODIS aerosol algorithm, products, and validation, J. Atmos. Sci., 62, 947–973, 2005.

Remer, L. A., Kleidman, R. G., Levy, R. C., Tanré, D., Mattoo, S., Vanderlei Martins, J., Ichoku, Ch., Koren, I., Yu, H., and Holben, B. N.: An emerging global aerosol climatology from the MODIS satellite sensors, J. Geophys. Res., 113, D14S07, doi:10.1029/2007JD009661, 2008.

Tanré, D., Kaufman, Y. J., Herman, M., and Mattoo, S.: Remote sensing of aerosol over oceans from EOS-MODIS, J. Geophys. Res., 102, 16971–16988, 1997.

Torres, O., Bhartia, P. K., Herman, J. R., Sinyuk, A., Ginoux, P., and Holben, B.: A Long-term record of aerosol optical depth from TOMS observations and comparison to AERONET measurements, J. Atmos. Sci., 59, 398–413, 2002.

Torres, O., Chen, Z., Jethva, H., Ahn, C., Freitas, S. R., and Bhartia, P. K.: OMI and MODIS observations of the anomalous 2008-2009 Southern Hemisphere biomass burning seasons, Atmos. Chem. Phys., 10, 3505–3513, doi:10.5194/acp-10-3505-2010, 2010.

AMTD
4, 2037–2069, 2011

Vanbauce, C., Cadet, B., and Marchand, R. T.: Comparison of POLDER apparent and corrected oxygen pressure to ARM/MMCR cloud boundary pressures, Geophys. Res. Lett., 30, 1212, doi:10.1029/2002GL016449, 2003.

Vaughan, M. A., Powell, K. A., Kuehn, R. E., Young, S. A., Winker, D. M., Hostetler, C. A., Hunt, W. H., Liu, Z., McGill, M. J., and Getzewich, B. J.: Fully Automated Detection of Cloud and Aerosol Layers in the CALIPSO Lidar Measurements, J. Atmos. Ocean. Tech., 26, 2034–2050, 2009.

Volten, H., Munoz, O., Rol, E., de Haan, J. F., Vassen, W., and Hovenier, J. W.: Scattering matrices of mineral aerosol particles at 441.6 nm and 632.8 nm, J. Geophys. Res., 106, 17375–17401, 2001.

Wang, M. and Gordon, H. R.: Radiance reflected from the ocean-atmosphere system: Synthesis from individual components of the aerosols size distribution, Appl. Optics, 33, 7088–7095, 1994.

Waquet, F., Riedi, J., Labonnote, L., Goloub, P., Cairns, B., Deuzé, J.-L., and Tanré, D.: Aerosol remote sensing over clouds using the A-Train observations, J. Atmos. Sci., 66(8), 2468–2480, 2009.

Waquet, F., Riedi, J., Labonnotte, L., Thieuleux, F., Ducos, F., Goloub, Ph., and Tanré, D.: Aerosols remote sensing over clouds using the A-train observations, A-Train Symposium, New Orleans, USA, 25–28 October, 2010.

Winker, D. M., Pelon, J., and McCormick, M. P.: The CALIPSO mission: Spaceborne lidarfor observation of aerosols and clouds, in: Lidar Remote Sensing for Industry and Environment Monitoring III, Proc. SPIE vol. 4893, edited by: Singh, U. N., Itabe, T., and Lui, Z., SPIE, Bellingham, WA, 1–11, 2003.

Winker, D. M., Vaughan, M. A., Omar, A., Hu, Y., Powell, K. A., Liu, Z., Hunt, W. H., and Young, V: Overview of the CALIPSO mission and CALIOP data processing algorithms, J. Atmos. Ocean. Tech., 26, 2310–2323, 2009.

Winker, D. M., Pelon, J., Coakley Jr., J. A., Ackerman, S. A., Charlson, R. J., Colarco, P. R., Flamant, P., Fu, Q., Hoff, R. M., Kittaka, C., Kubar, T. L., LeTreut, H., McCormick, M. P., Mégie, G., Poole, L., Powell, K., Trepte, C., Vaughan, M. A., and Wielicki, B. A.: The CALIPSO mission: a global 3D view of aerosols and clouds, B. Am. Meteorol. Soc., 91, 1211–1229, doi:10.1175/2010BAMS3009.1, 2010.

AMTD
4, 2037–2069, 2011

Table 1. List of the aerosol parameters currently derived from the PARASOL operational algorithms : over ocean (τ_{tot} = total aerosol optical thickness; r_{eff} = effective radius of the aerosol size distribution; m_r = real part of the refractive index of the aerosol fine mode; α = angstrom exponent for total aerosol optical thickness; τ_{acc} = optical thickness of the aerosol fine mode; $\tau_{c,ns}$ = optical thickness for large nonspherical aerosols) and over land ($\tau_{acc,land}$ = optical thickness of the aerosol fine mode). The spatial resolution is $18.5 \times 18.5\,km^2$ and the parameters are vertically integrated.

Retrieved quantity	Typical accuracy	Retrieval algorithm reference	Validation reference
τ_{tot}	$\pm 0.05\,\tau \pm 0.05$	Deuzé et al. (1999)	Goloub et al. (1999)
r_{eff}	Fine: 0.05 µm Coarse: 0.5 µm	Herman et al. (2005)	TBC
m_r	0.10	Herman et al. (2005)	TBC
α	0.3–0.5	Deuzé et al. (1999)	Goloub et al. (1999)
τ_{acc}	TBD	Herman et al. (2005)	Bréon et al. (2010)
$\tau_{c,ns}$	TBD	Herman et al. (2005)	TBC
$\tau_{acc,land}$	TBD	Deuzé et al. (2001)	Fan et al. (2008)

AMTD
4, 2037–2069, 2011

Table A1. Size distribution parameters of the aerosol models over ocean. m_r and m_i are the real and imaginary parts of the refractive index. For the non-spherical mode, the phase matrix is directly obtained from Volten et al. (2001); the size parameters r_0 and σ_0 are assumed equal to the values of the spherical coarse mode; no values are assigned for the refractive index. The non-spherical fraction within the coarse mode is set to 5 discrete values: 0.00, 0.25, 0.50, 0.75 and 1.00.

	r_0 (µm)	σ_0	r_{eff} (µm)	m_r	m_i
Fine Mode	0.04, 0.08, 0.10, 0.13	0.46	0.068, 0.136, 0.169, 0.220	1.35, 1.45, 1.60	0.00
Spherical Coarse Mode	0.75	0.69	2.55	1.33, 1.35, 1.37	0.00
Non-Spherical Coarse Mode	0.75	0.69	2.55	Not Defined	Not Defined

AMTD
4, 2037–2069, 2011

Table A2. Size distribution parameters of the aerosol models over land. m_r and m_i are the real and imaginary parts of the refractive index. Coarse particles are not included in the LUT.

	r_0 (µm)	σ_0	r_{eff} (µm)	m_r	m_i
Fine Mode	0.05, 0.06, 0.07, 0.08, 0.09, 0.10, 0.11, 0.12, 0.13, 0.15	0.40	0.075, 0.090, 0.105, 0.120, 0.135, 0.150, 0.165, 0.180, 0.195, 0.225	1.47	0.01
Spherical Coarse Mode	Not Defined	Not Defined	Not Defined	Not Defined	Not Defined
Non-Spherical Coarse Mode	Not Defined	Not Defined	Not Defined	Not Defined	Not Defined

AMTD
4, 2037–2069, 2011

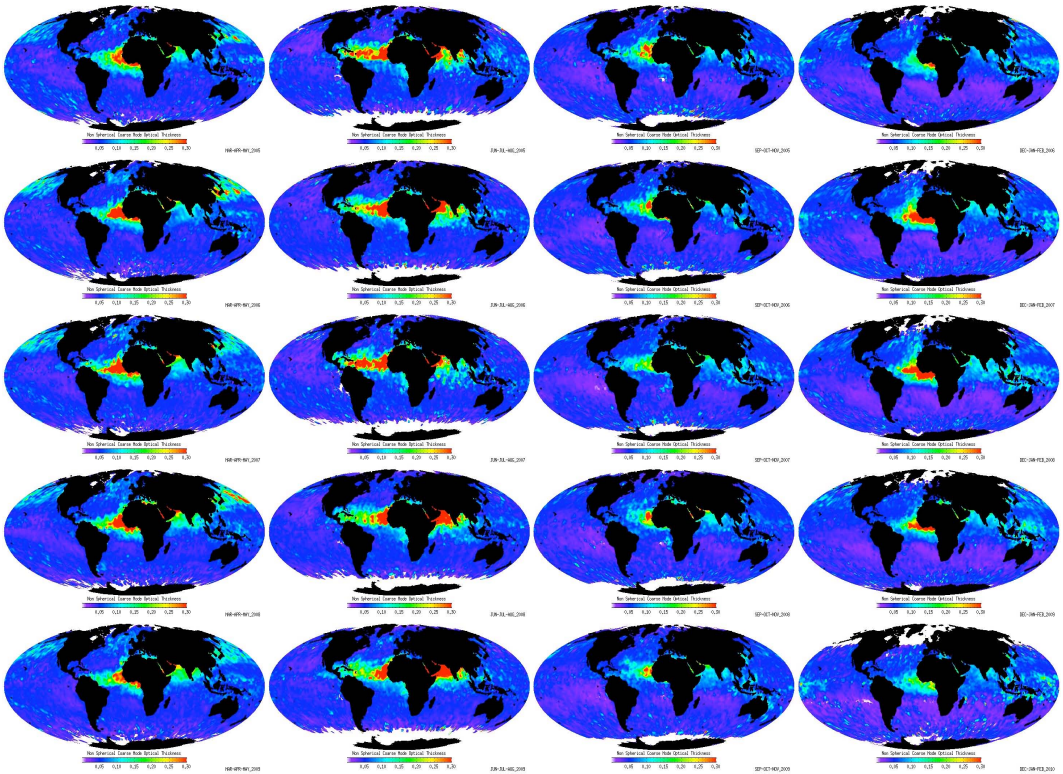

Fig. 1. AOD at 550 nm resulting from the non-spherical particles in the coarse mode. Seasons are ordered from the left to the right (spring, summer, autumn, winter), years from the top to the bottom (from 2005 to 2010).

AMTD
4, 2037–2069, 2011

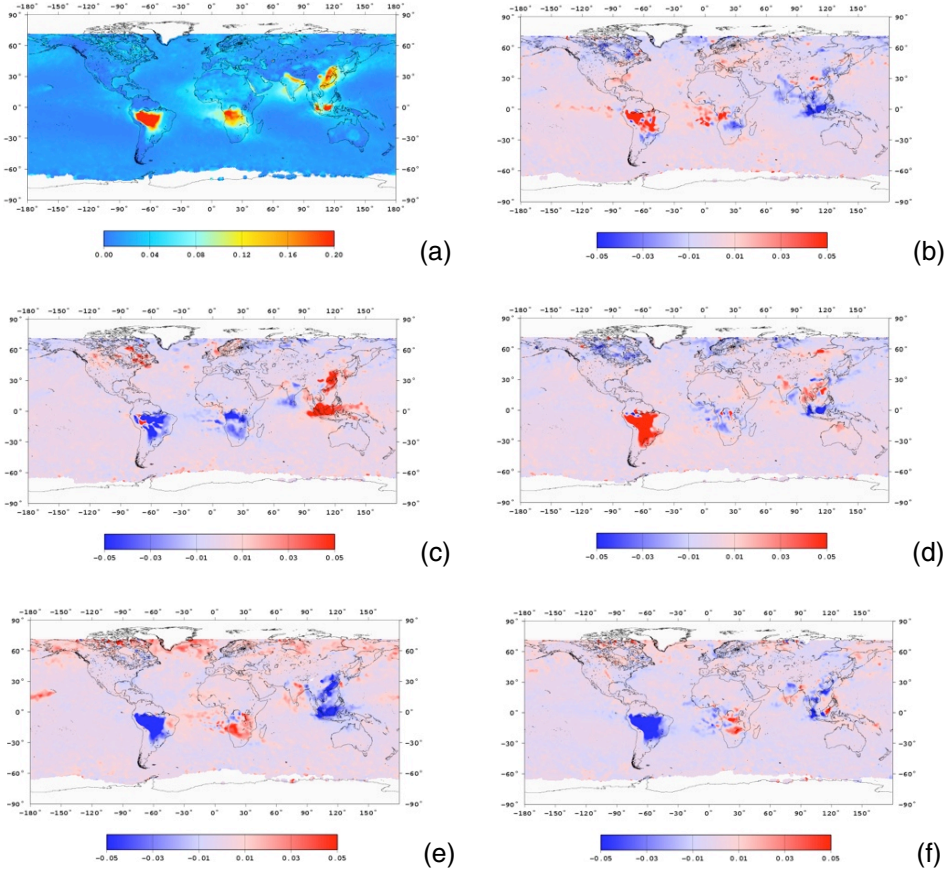

Fig. 2. (a) AOD at 550 nm resulting from the accumulation mode averaged over three months September-October-November and the 5 years. **(b)–(f)** AOD anomalies for the 5 years from 2005 to 2009 respectively. Blues indicate that the AOD of the year was lower than the long term mean and reds indicate higher values.

AMTD
4, 2037–2069, 2011

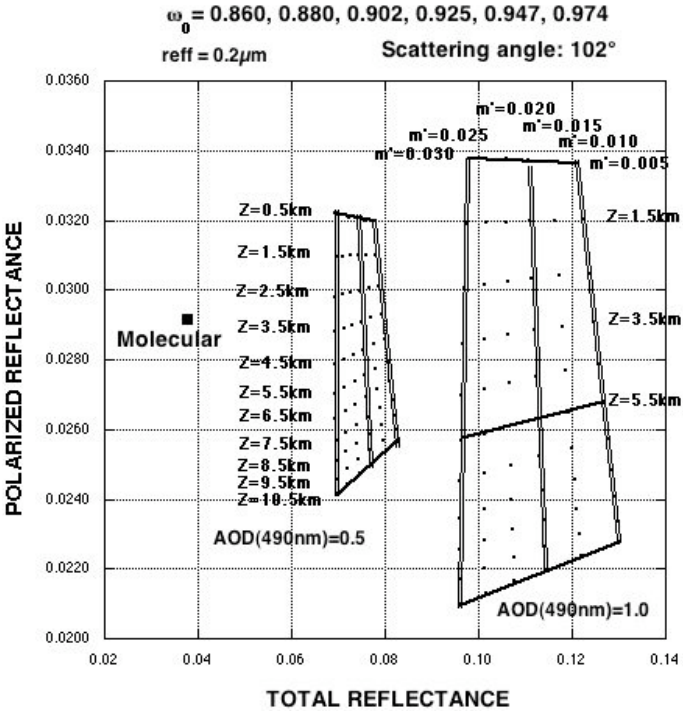

Fig. 3. Scatter plot of the polarized (y-axis) and total (x-axis) radiances at 0.490 µm. Solid lines represent the polarized radiances that are measured for one value of the altitude layer (0.5 km to 10.5 km with a step of 0.5 km) and different absorptions (imaginary part of the refractive index from 5.0×10^{-3} to 3.0×10^{-2}) which corresponds to a single sacttering albedo of 0.974, 0.947, 0.925, 0.902, 0.880 and 0.860 respectively. A double-line represents the total radiances that are measured for one value of the absorption and different altitude layers. Three values of the optical depth (0.0, 0.5 and 1.0) are reported; AOD = 0.0 corresponds to a molecular atmosphere as the reference. Observations conditions correspond to scattering angle of 102° and a standart fine mode aerosol r_{eff} = 0.2 µm.

AMTD
4, 2037–2069, 2011

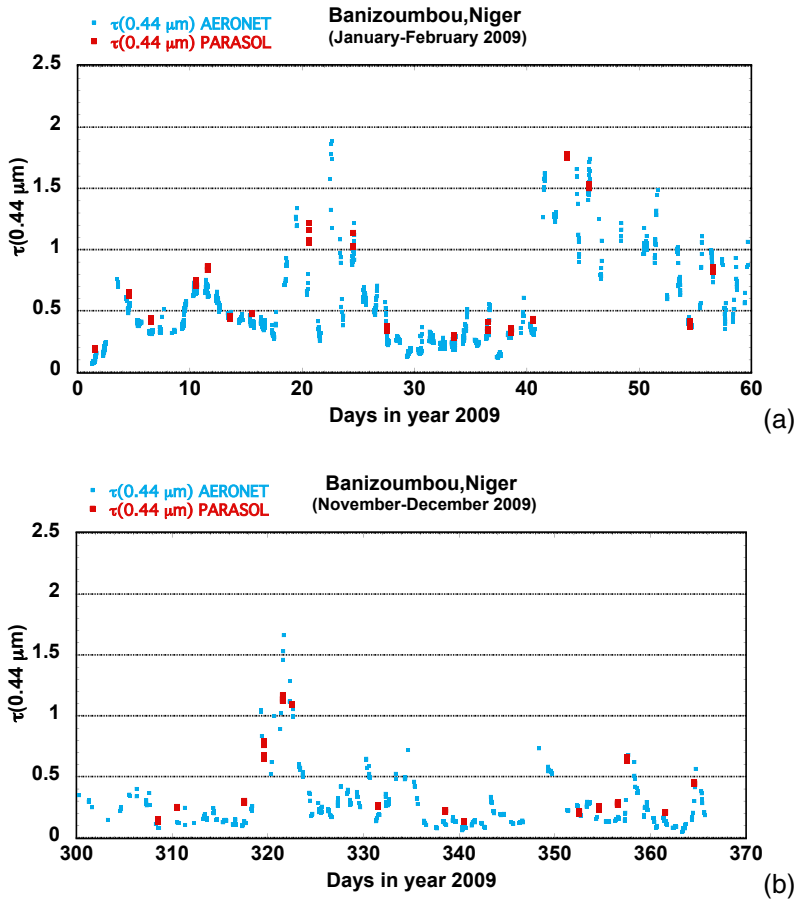

Fig. 4. **(a)** Comparison of τ (0.44 µm) retrieved from POLDER/PARASOL during January–February 2009 over Banizoumbou/Niger with the corresponding values provided by AERONET. **(b)** Same as **(a)** for the November–December period.

AMTD
4, 2037–2069, 2011